



**High-energy velocity tails in uniformly heated granular materials**Yangrui Chen <sup>1</sup> and Jie Zhang <sup>1,2,\*</sup><sup>1</sup>*School of Physics and Astronomy, Shanghai Jiao Tong University, Shanghai 200240, China*<sup>2</sup>*Institute of Natural Sciences, Shanghai Jiao Tong University, Shanghai 200240, China*

(Received 4 July 2022; accepted 17 November 2022; published 30 November 2022)

We experimentally investigate the velocity distributions of quasi-two-dimensional granular materials uniformly heated by an electromagnetic vibrator, where the translational velocity and the rotation of a single particle are Gaussian and independent. We observe the non-Gaussian distributions of particle velocity, with the density-independent high-energy tails characterized by an exponent of  $\beta = 1.50 \pm 0.03$  for volume fractions of  $0.111 \leq \phi \leq 0.832$ , covering a wide range of structures and dynamics. Surprisingly, our results are not only in excellent agreement with the prediction of the kinetic theories of granular gas but also hold for an extremely high-volume fraction of  $\phi = 0.832$  where the granular material forms a crystalline solid and the kinetic theory of granular gas fails fantastically. Our experiment suggests that the density-independent high-energy velocity tails of  $\beta = 1.50$  are a characteristic of uniformly heated granular matter.

DOI: [10.1103/PhysRevE.106.L052903](https://doi.org/10.1103/PhysRevE.106.L052903)

**Introduction.** Due to inelastic collisions [1–3], a granular gas may exhibit rich behaviors drastically different from those of a molecular gas [4–6], such as clustering [4,7–10], collective motions [11–15], phase separations [16–19], and non-Gaussian velocity distributions [20–23]. The study of granular gas is important for a large variety of fields, including the glass and jamming transitions [24–27], the collective motions of active matter [12,28,29], and the applications in chemical engineering [30], in meteorology [31], and in astrophysics [32].

One of the distinct characteristics of a granular gas is the high-energy tails of its velocity distributions. Based on the Enskog-Boltzmann equation, the kinetic theories [1,22,33–37] predict that the velocity distributions are non-Gaussian, exhibiting density-independent high-energy velocity tails  $P(v) \propto \exp(-c \times (v/|v|)^\beta)$ . Here  $c$  is a constant related to inelasticity, and  $\beta = 1$  for homogeneous cooling states and  $\beta = 1.5$  for homogeneous driving states, in which the corresponding theories are formulated on the same mathematics [1,22,33–37]. The predicted values of  $\beta$  have been successfully reproduced in the state-of-the-art numerical works [20,34,38–41].

It is a great challenge to test the theories [1,22,33–37] in experiments. The values of  $\beta = 1.0$  and  $\beta = 1.5$  have been reported in a number of experiments [28,42–49], which, however, are not exactly in line with the theoretical setup and predictions [1,22,33–37]. In the three-dimensional (3D) systems driven by a uniform magnetic field along the gravitational direction [46,47], the tails of the distributions of horizontal velocity components are density independent with  $\beta = 1$  instead of 1.5, which is attributed to the anisotropy of driving and gravity and is similarly observed in Ref. [49]. In the quasi-two-dimensional (2D) vertical systems subject

to boundary driving, there is spatial heterogeneity along the vertical direction [45,48]. Consequently, the results are analyzed for particles around the midheight of the systems [45,48]. In the quasi-2D horizontal layers of beads subject to homogeneous vertical shaking [9,44,48], different values of  $\beta$  are reported in similar setups depending on the third dimension of a system, suggesting an important role of 3D effects. Interestingly,  $\beta \approx 1.5$  is observed in a plasmalike dilute quasi-2D horizontal layer of beads with long-range electrostatic interactions [50], where the value of  $\beta$  may also depend on the driving frequency as further revealed in the numerical simulations [50]. In a 2D layer of homogeneously driven *Vibrot* particles [28], the velocity distributions exhibit high-energy tails of  $\beta \approx 1.50$  for volume fractions of 0.47 and 0.6. However, *Vibrot* particles excite translational motion through the coupling to the unidirectional rotation, which breaks the time-reversal symmetry and behaves more like active matter and whose volume fractions are also above the regime of granular gas.

In this Letter, we design the vibration-driven Brownian particles (VBPs) to investigate the velocity distributions of the homogeneously driven quasi-2D granular systems from the dilute gases to the ultradense limit of granular crystals, covering a broad range of volume fractions of  $0.111 \leq \phi \leq 0.832$ , in which the volume fraction  $\phi$  refers to the ratio between the area covered by all particles and the total area of a 2D system. We show that the non-Gaussian velocity distributions exhibit robust density-independent high-energy tails with  $\beta = 1.5 \pm 0.03$  for all volume fractions. Our results are not only in excellent agreement with the prediction of the kinetic theories of granular gas but also hold for granular crystal solids at  $\phi = 0.832$  where the kinetic theory of granular gas fails fantastically. This surprising agreement suggests that the predictions of the kinetic theory of granular gas are very general, regardless of the detailed structures and dynamics as well as the overall volume fraction.

\*jiezhang2012@sjtu.edu.cn

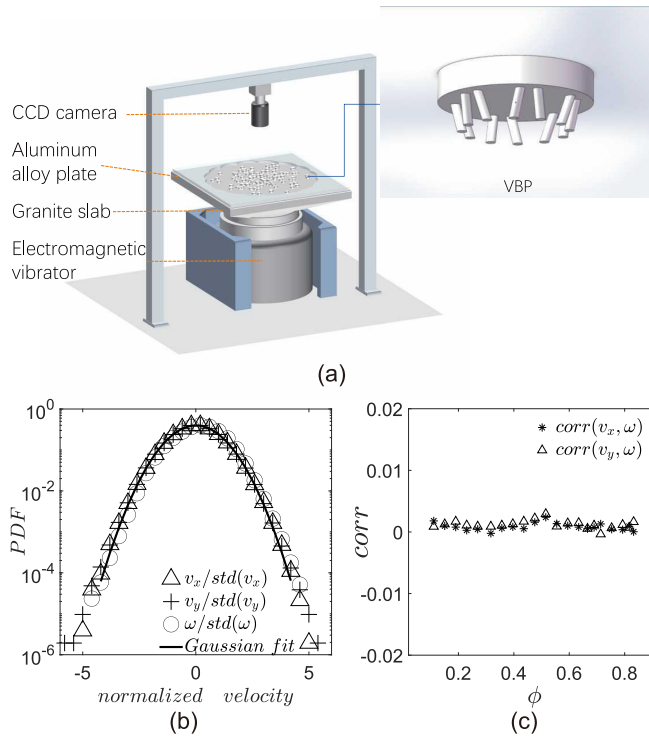


FIG. 1. (a) Schematic of the experimental setup. The inset shows that VBP is a disk with 12 alternately inclined supporting legs. The diameter of the disk is  $D = 16$  mm and the thickness is 3 mm. The legs with a height of 3 mm are inclined inward by  $18.4^\circ$  and alternately deviated from the midaxis plane by  $\pm 38.5^\circ$ . We use a black marker to draw a line on the surface of each disk to identify its orientation. (b) The normalized velocity distributions of the translational components  $v_x$  and  $v_y$  and the rotational component  $\omega$  of a single VBP. (c) The Pearson correlation coefficients between  $v_x$  and  $\omega$  and between  $v_y$  and  $\omega$ , showing the translational and rotational motions of the single VBP are independent.

**Experimental setup.** Our experimental system is a horizontal layer of quasi-2D monodisperse granular materials driven homogeneously by an electromagnetic vibrator as shown in Fig. 1(a). The electromagnetic vibrator drives vertically a whole piece of granite with a top flat surface ( $60 \text{ cm} \times 60 \text{ cm}$ ) of a weight of 60 kg. The rigidity of granite effectively suppresses potential standing waves on the top flat surface. A flat aluminum alloy plate ( $60 \text{ cm} \times 60 \text{ cm} \times 1 \text{ cm}$ ) is mounted onto the granite by eight strong F-clamps. An acrylic sheet is cut into a flower-shaped lateral boundary as used in Refs. [12,51] to reinject creeping particles into the interior to suppress creep particle motions along the boundary [52].

The electromagnetic vibrator provides sinusoidal vibration with the frequency  $f = 100$  Hz and the maximum acceleration  $a = 3g$ , where  $g$  is the gravitational acceleration. The amplitude  $A \equiv a/(2\pi f)^2 = 0.074$  mm, and thus the particle displacement in the vertical direction is negligible compared to the horizontal displacement. We carefully control the vibrator to ensure that the granular system has no obvious gravitational drift within 6 h of continuous vibration. The results presented here are not affected by the different choices of the values of  $a$  and  $f$ , e.g., if we keep  $f = 100$  Hz fixed and change  $a$  within  $2.6g < a < 3.2g$ , we observe the values

of  $\beta \approx 1.5$  and the qualitatively same behaviors in flow patterns and dynamics, and alternatively, if we keep  $a = 3g$  fixed and change  $f$  within  $80 \text{ Hz} < f < 120 \text{ Hz}$ , we observe the similar behaviors. When the increase of  $a$  or the decrease of  $f$  goes beyond the aforementioned ranges, 3D effects become apparent, such as the particle tilting and the occasion of the particle flipping upside down. Conversely, when the decrease of  $a$  or the increase of  $f$  goes beyond the aforementioned ranges, particle motions may become significantly reduced.

In each experiment, we first place a given number of VBPs randomly and uniformly on the base plate and apply vibration for 2 h to obtain an initial state. We then use a Basler CCD camera (acA2040-180kc) above to capture particle configurations and to track particle motions at 40 frames/s for 1 h. We repeat each experimental run three times to take an ensemble average for an array of volume fractions  $\phi$  ranging from 0.111 to 0.832 in an equal interval of 0.040. Finally, we identify and track the positions and orientations of particles using image-processing software. We discard the particles within three layers next to the boundary to eliminate potential boundary effects.

**Single VBP.** The velocity distribution of a flat-bottomed disk on a smooth vibrating surface is non-Gaussian [43]. Inspired by Vibrot particles introduced by Altshuler *et al.* [53] and Scholz *et al.* [54], we design an alternative vibration-driven Brownian particle (VBP) shown in the inset of Fig. 1(a), whose legs are inclined inward to prevent stumble with alternately tilted angles between two neighboring legs to effectively randomize the motion of the particle with respect to the flat surface. Before a leg bounces onto the vibrating plate, a single VBP performs a quasiballistic motion with an average time of  $\tau_b \approx 38$  ms, which is slightly longer than the sampling interval  $\tau_{si} = 25$  ms. Altogether, we have a maximum of 1100 VBPs which are 3D printed with CBY-01 resin.

**Velocity distributions.** For a single VBP, the distributions of the rotational velocity  $\omega$  and the translational velocity components  $v_x$  and  $v_y$  are shown in Fig. 1(b). All curves are normalized by their standard deviations. The results fit perfectly with the Gaussian distribution represented by the solid line with a mean value  $|\mu| < 0.1$ , which means that the motion of a single VBP is both random and isotropic. For different VBPs, their  $\mu$ 's fluctuate very near zero. In Fig. 1(c), we confirm that the translation and rotation are completely independent. Thus, VBP is a suitable model for uniformly driven quasi-2D granular materials, analogous to a uniformly heated thermal system.

Our main goal is to measure the velocity distributions of the uniformly heated granular materials and compare them with the predictions of kinetic theory [1,22,33–37]. The velocity distributions of different volume fractions  $\phi$  are shown in the main panel of Fig. 2. Here we only plot the curves for a selected set of  $\phi$  in the main panel of Fig. 2 to avoid overclouded curves. All curves follow the similar stretched exponential fat tails on the semilog plot, where the solid lines guide the eye with the fitting of the stretched exponential form  $\propto \exp(-c \times (v/|v|)^\beta)$ . To fit the tails, we choose the range of fitting to be  $v/|v| \geq 2$ , as marked by the vertical dashed line  $(v/|v|)^{1.5} \approx 2.83$  in Fig. 2. However, the values of fitting parameters are insensitive to the actual starting position of the dashed line. The fluctuation of the characteristic velocity  $|v|$

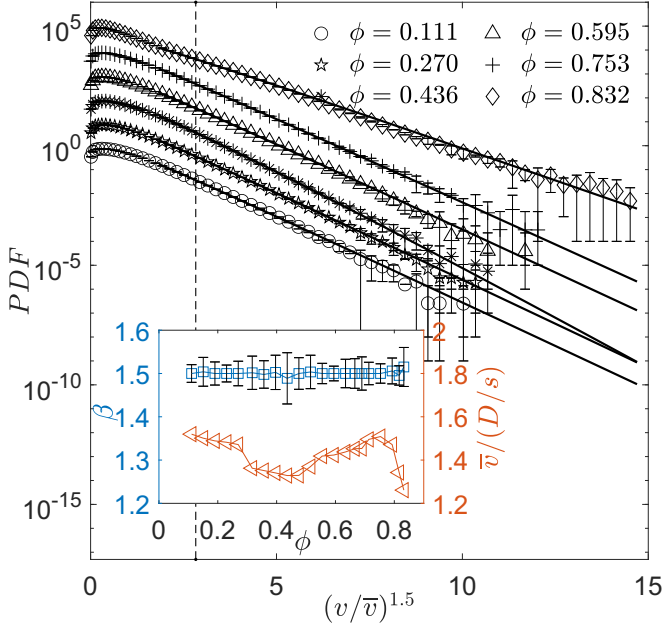


FIG. 2. Velocity distributions. The horizontal axis represents the normalized velocity  $(v/|v|)^{1.5}$  with  $v = \sqrt{v_x^2 + v_y^2}$ , where  $|v|$  is the characteristic velocity corresponding to  $\langle \frac{1}{2}v^2 \rangle$  averaged over both space and time. The error bars are estimated from three independent repeated experiments. A set of representative curves are consecutively shifted upwards by a factor of 10 to enhance visibility. The solid lines are drawn as a guide to the eye, representing the nonlinear fitting. The starting point of the fit is marked with a dashed line at  $v/|v| = 2$ . The inset shows the fitting coefficients  $\beta$  (blue square) and the characteristic velocity  $|v|$  [orange triangle, unit: particle diameter per second (D/s)] for all volume fractions  $\phi$ .

with the volume fraction is very limited as shown in the inset of Fig. 2. Although the parameter  $c$  varies with volume fraction as shown in Table I, the values of the stretched exponent  $\beta$  are all around 1.5, in excellent but surprising agreement with the prediction of the kinetic theory [1,22,33–37]. The values of  $\beta$  within a wide range of volume fractions, i.e.,  $0.111 \leq \phi \leq 0.832$ , are shown in the inset of Fig. 2, showing the consistent values of  $\beta = 1.5 \pm 0.03$ . This fantastic agreement is rather surprising for two reasons: first, the particle dynamics and configurations depend strongly on the volume fraction  $\phi$ ; second, the dense regime where  $\phi \geq 0.7$  goes beyond the typically applicable regime of the kinetic theory of granular gas [1,22,33–37].

In an early experiment, a layer of stainless-steel beads is shaken vertically on the plate of an electric vibrator [9]: when the shaking is gentle such that the beads remain quasi-2D with no particle crossing through the third dimension, the high-energy velocity tails are exponentially distributed for a low-volume fraction and a high-volume fraction, qualitatively

different from our results. We are not sure of the exact cause of such exponential distributions, but we suspect that the velocity distributions of a single stainless-steel bead may not be Gaussian, similar to a single flat-bottomed disk [43]. In a similar experiment [44], when the shaking is sufficiently strong such that the driven stainless-steel beads are quasi-3D, with all beads confined within the five-particle-diameter space vertically by a top glass cover, the distributions of the horizontal velocity components show high-energy tails of  $\beta \approx 1.5$  [44]. It is clear that the 3D effect is important for the  $\beta \approx 1.5$  results [44]: when the shaking strength is tuned down to recover a quasi-2D system, the high-energy tails of velocity distributions become exponentially distributed, in agreement with the results seen in Ref. [9]. In another experiment of similar geometry [48],  $\text{ZnO}_2$  beads are confined between a rough top cover and a flat-bottom plate with an average thickness of 1.8 particle diameters within a cylindrical cell. When the cell is subject to vertical vibrations, the horizontal velocities also show high-energy tails of  $\beta \approx 1.5$  [48]. However, it is unclear how important the 3D effect is and whether the distribution of a single particle is itself non-Gaussian in Ref. [48].

The results in Fig. 2 are nontrivial as can be seen from the qualitatively different dynamics at different volume fractions  $\phi$ . Figures 3(a)–3(c) show the typical particle configurations along with the respective instantaneous velocity fields, i.e., the displacement field over the shortest time interval of 25 ms for three different volume fractions  $\phi$ . Here the arrows are magnified 20 times for better visibility. For all three  $\phi$ 's, the instantaneous velocity fields are spatially random despite that at different  $\phi$ 's the particle configurations are quite different. At the relatively low-volume fraction  $\phi = 0.270$ , the particle configurations are more heterogeneous and sparse with chainlike structures mingled with empty space. At the higher-volume fraction  $\phi = 0.555$ , the particle configurations are more uniform in space. At  $\phi = 0.832$ , the particles fill up the whole space in crystalline structures except near the boundary and become solid. Figures 3(d)–3(f) show the corresponding displacement fields at a much longer interval of 10 min. At  $\phi = 0.270$  the displacement field is still spatially random as shown in Fig. 3(d), similar to the one in Fig. 3(a). However, at  $\phi = 0.555$  the displacement field shows a collective swarming motion in Fig. 3(e), similar to those observed in the active matter system [29]. At  $\phi = 0.832$  the long-interval displacement field is negligibly small, consistent with the crystalline structures. It is remarkable that with the increase of  $\phi$  the particle configurations and dynamics change drastically but the velocity distributions nonetheless show robust density-independent high-energy tails of the same exponent  $\beta = 1.5 \pm 0.03$ .

In order to verify the spatially uniform energy input, we first coarse-grain the bottom surface with the grid size of  $0.1D$ , where  $D = 16$  mm refers to the diameter of a VBP, and then draw the color map of the ensemble means of  $|v_{\text{local}}|/v_{\text{global}}$  in Figs. 3(d)–3(f). Here  $|v_{\text{local}}|$  is the local velocity magnitude at

TABLE I. The fitting parameter  $c$  versus the volume fraction  $\phi$ .

|        |       |       |       |       |       |       |       |       |       |       |       |       |       |       |       |       |       |       |       |       |
|--------|-------|-------|-------|-------|-------|-------|-------|-------|-------|-------|-------|-------|-------|-------|-------|-------|-------|-------|-------|-------|
| $\phi$ | 0.111 | 0.151 | 0.190 | 0.230 | 0.270 | 0.317 | 0.357 | 0.396 | 0.436 | 0.476 | 0.515 | 0.555 | 0.595 | 0.634 | 0.690 | 0.713 | 0.753 | 0.793 | 0.817 | 0.832 |
| $c$    | 4.695 | 4.632 | 4.870 | 4.860 | 4.975 | 6.364 | 6.616 | 6.444 | 7.634 | 5.401 | 4.805 | 4.444 | 4.521 | 4.549 | 4.957 | 4.624 | 4.300 | 3.177 | 2.291 | 1.474 |

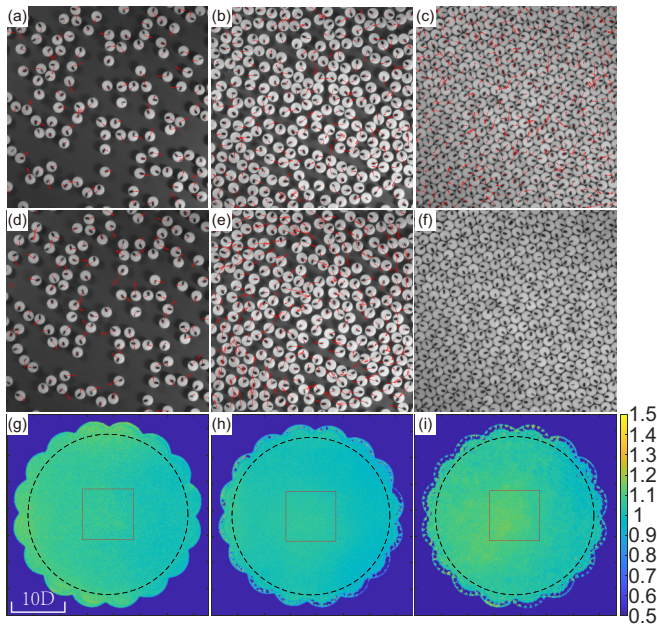


FIG. 3. (a)–(c) Three zoomed representative particle configurations at volume fractions  $\phi = 0.270$ ,  $0.555$ , and  $0.832$ . The red arrows depict the individual particle’s displacement vector over 25 ms. Here, the arrow size is magnified 20 times from its original size. (d)–(f) The zoomed particle configurations are the same as panels (a)–(c) except that the red arrows now represent the particle displacement fields over 10 min. Here, the arrow size is reduced to 0.1 times its original size. (g)–(i) The local speed map at  $\phi = 0.270$ ,  $0.555$ , and  $0.832$  showing spatially uniform driving, the color represents the time average of  $|v_{\text{local}}|/v_{\text{global}}$ , where the  $v_{\text{local}}$  is the local velocity at a given time, i.e., the displacement over consecutive frames of time interval 25 ms, and  $v_{\text{global}}$  is the square root of the spatial average of  $v_{\text{local}}^2$ . The black dashed circles indicate the particle configurations excluding boundaries and the red squares correspond to the regimes of panels (a)–(f).

a given time, i.e. the magnitude of displacement between two consecutive frames of the time interval of 25 ms, and  $v_{\text{global}}$  is the square root of the spatial average of  $v_{\text{local}}^2$ . After the exclusion of the outermost three particle layers, the fluctuations of  $|v_{\text{local}}|/v_{\text{global}}$  are within  $4.5\% \sim 6.7\%$ . We change the coarse-grain scale from  $0.1D$  to  $0.5D$ , and the results are consistent. A similar uniform heating is also observed in the 2D homogeneously driven Vibrot particles [28]. In an early experiment, where a quasi-2D vertical cell filled with a small fraction of stainless-steel beads is subject to vertical vibrations at the bottom wall, the distribution of the horizontal velocities is given by  $P(v) \propto \exp(-c \times |v|^\beta)$ , with  $\beta$  around 1.5 [45]. However, the boundary-driven systems typically suffer from strong spatial inhomogeneity, e.g., for the density and

velocities along the vertical direction under normal gravity [45] or microgravity [48], and the results are thus only analyzed within a horizontal strip centered around the midheight of the cell [45,48]. Thus, our system is indeed subject to a spatially uniform energy input, which we believe is the key to our successful observation of the high-energy velocity tails with the predicted exponent of  $\beta = 1.5 \pm 0.03$  for all volume fractions.

Our density-independent high-energy velocity tails of  $\beta = 1.5$  go far beyond the scope of the kinetic theories of granular gas [1,22,33–37]. Moreover, the coefficient  $c$  is density dependent and thus nonuniversal. To fully understand our results clearly requires new theories to be developed. The kinetic theories [1,22,33–37] that lead to the prediction of the exponent of  $\beta = 1.5$  contain two essential ingredients as follows, which we believe are crucial in developing new theories in the future. First, despite that kinetic energy is not conserved, momentum, or equivalently velocity, is still conserved during collisions; each collision tries to preserve the direction and magnitude of the incoming particle’s velocity if its speed is much larger than that of its collision particle. Second, there exists uniform heating, which is equivalent to the random walk of each particle in its velocity subspace. In the case of the homogeneous cooling of granular gases in the absence of uniform heating, the kinetic theories predict an exponential distribution for the high-energy velocity tail [1,22,33–37]. In the presence of the uniform heating [1,22,33–37], the high-energy tails of velocity distributions become a stretched exponential of an exponent of  $\beta = 1.5$  considering the additional contribution of the random walk of each particle in its velocity subspace.

**Conclusion.** We have built an alternative system by using the vibration-driven Brownian particles to investigate the velocity distributions of the homogeneously driven quasi-2D granular materials, subject to a uniform energy input analogous to the uniformly heated thermal systems. Our system provides consistent results across the wide range of volume fractions of  $0.111 \leq \phi \leq 0.832$ , which convincingly support that the velocity distributions exhibit the density-independent high-energy tails  $\propto \exp(-c \times (v/|v|)^\beta)$ , where  $\beta = 1.5 \pm 0.03$  regardless of the structures of the particles configurations and detailed dynamical behaviors. These nontrivial results are much more general than the scope of the kinetic theory of granular gases, suggesting that the density-independent high-energy tails are the fundamental characteristics of the uniformly heated granular materials.

Y.C. and J.Z. acknowledge the support from the NSFC (Grant No. 11974238) and the Innovation Program of Shanghai Municipal Education Commission under Grant No. 2021-01-07-00-02-E00138. Y.C. and J.Z. also acknowledge the support from the Student Innovation Center of Shanghai Jiao Tong University.

- [1] V. Garzó, *Granular Gaseous Flows* (Springer, Cham, 2019).  
 [2] A. Puglisi, *Transport and Fluctuations in Granular Fluids: From Boltzmann Equation to Hydrodynamics, Diffusion and Motor Effects* (Springer, Berlin, 2014).

- [3] C. S. Campbell, *Annu. Rev. Fluid Mech.* **22**, 57 (1990).  
 [4] S. E. Esipov and T. Pöschel, *J. Stat. Phys.* **86**, 1385 (1997).  
 [5] L. P. Kadanoff, *Rev. Mod. Phys.* **71**, 435 (1999).  
 [6] S. R. Nagel, *Rev. Mod. Phys.* **89**, 025002 (2017).

- [7] I. Goldhirsch and G. Zanetti, *Phys. Rev. Lett.* **70**, 1619 (1993).
- [8] M. Noirhomme, F. Ludewig, N. Vandewalle, and E. Opsomer, *Phys. Rev. E* **95**, 022905 (2017).
- [9] J. S. Olafsen and J. S. Urbach, *Phys. Rev. Lett.* **81**, 4369 (1998).
- [10] M. X. Lim, A. Souslov, V. Vitelli, and H. M. Jaeger, *Nat. Phys.* **15**, 460 (2019).
- [11] A. Bricard, J.-B. Caussin, D. Das, C. Savoie, V. Chikkadi, K. Shitara, O. Chepizhko, F. Peruani, D. Saintillan, and D. Bartolo, *Nat. Commun.* **6**, 7470 (2015).
- [12] J. Deseigne, O. Dauchot, and H. Chaté, *Phys. Rev. Lett.* **105**, 098001 (2010).
- [13] P. Eshuis, K. van der Weele, D. Lohse, and D. van der Meer, *Phys. Rev. Lett.* **104**, 248001 (2010).
- [14] P. Liu, H. Zhu, Y. Zeng, G. Du, L. Ning, D. Wang, K. Chen, Y. Lu, N. Zheng, F. Ye *et al.*, *Proc. Natl. Acad. Sci. USA* **117**, 11901 (2020).
- [15] B. Zhang, H. Yuan, A. Sokolov, M. O. de la Cruz, and A. Snezhko, *Nat. Phys.* **18**, 154 (2022).
- [16] J. G. Downs, N. D. Smith, K. K. Mandadapu, J. P. Garrahan, and M. I. Smith, *Phys. Rev. Lett.* **127**, 268002 (2021).
- [17] L.-H. Luu, G. Castillo, N. Mujica, and R. Soto, *Phys. Rev. E* **87**, 040202(R) (2013).
- [18] K. Roeller, J. P. D. Clewett, R. M. Bowley, S. Herminghaus, and M. R. Swift, *Phys. Rev. Lett.* **107**, 048002 (2011).
- [19] M. Noirhomme, A. Cazaubiel, E. Falcon, D. Fischer, Y. Garrabos, C. Lecoutre-Chabot, S. Mawet, E. Opsomer, F. Palencia, S. Pillitteri, and N. Vandewalle, *Phys. Rev. Lett.* **126**, 128002 (2021).
- [20] X. Nie, E. Ben-Naim, and S. Chen, *Phys. Rev. Lett.* **89**, 204301 (2002).
- [21] S. N. Pathak, Z. Jabeen, D. Das, and R. Rajesh, *Phys. Rev. Lett.* **112**, 038001 (2014).
- [22] T. P. C. van Noije and M. H. Ernst, *Granular Matter* **1**, 57 (1998).
- [23] A. Megías and A. Santos, *Granular Matter* **21**, 49 (2019).
- [24] A. S. Keys, A. R. Abate, S. C. Glotzer, and D. J. Durian, *Nat. Phys.* **3**, 260 (2007).
- [25] K. Watanabe and H. Tanaka, *Phys. Rev. Lett.* **100**, 158002 (2008).
- [26] A. Seguin and O. Dauchot, *Phys. Rev. Lett.* **117**, 228001 (2016).
- [27] H. Xiao, A. J. Liu, and D. J. Durian, *Phys. Rev. Lett.* **128**, 248001 (2022).
- [28] C. Scholz and T. Pöschel, *Phys. Rev. Lett.* **118**, 198003 (2017).
- [29] S. Ramaswamy, *J. Stat. Mech.: Theory Exp.* (2017) 054002.
- [30] L.-S. Fan and C. Zhu, *Principles of Gas-Solid Flows* (Cambridge University, Port Chester, NY, 1999).
- [31] X. Wang, Z. Dong, J. Zhang, and L. Liu, *J. Arid Environ* **58**, 559 (2004).
- [32] J. Bouwman, T. Henning, L. Hillenbrand, M. Meyer, I. Pascucci, J. Carpenter, D. Hines, J. Kim, M. Silverstone, D. Hollenbach *et al.*, *Astrophys. J.* **683**, 479 (2008).
- [33] N. V. Brilliantov and T. Pöschel, *Kinetic Theory of Granular Gases* (Oxford University Press on Demand, New York, 2004).
- [34] T. Pöschel, N. V. Brilliantov, and A. Formella, *Phys. Rev. E* **74**, 041302 (2006).
- [35] V. Prasad, D. Das, S. Sabhapandit, and R. Rajesh, *J. Stat. Mech.: Theory Exp.* (2019) 063201.
- [36] V. Prasad and R. Rajesh, *J. Stat. Phys.* **176**, 1409 (2019).
- [37] A. Zippelius, *Phys. A (Amsterdam, Neth.)* **369**, 143 (2006).
- [38] J. S. van Zon and F. C. MacKintosh, *Phys. Rev. Lett.* **93**, 038001 (2004).
- [39] J. J. Brey, D. Cubero, and M. J. Ruiz-Montero, *Phys. Rev. E* **59**, 1256 (1999).
- [40] J. J. Brey and M. Ruiz-Montero, *Comput. Phys. Commun.* **121-122**, 278 (1999).
- [41] A. Puglisi, V. Loreto, U. Marini Bettolo Marconi, and A. Vulpiani, *Phys. Rev. E* **59**, 5582 (1999).
- [42] P. Yu, M. Schröter, M. Adachi, and M. Sperl, *EPJ Web Conf.* **249**, 04002 (2021).
- [43] L. Guan, L. Tian, M. Hou, and Y. Han, *Sci. Rep.* **11**, 16561 (2021).
- [44] W. Losert, D. Cooper, J. Delour, A. Kudrolli, and J. Gollub, *Chaos* **9**, 682 (1999).
- [45] F. Rouyer and N. Menon, *Phys. Rev. Lett.* **85**, 3676 (2000).
- [46] E. Falcon, J.-C. Bacri, and C. Laroche, *Europhys. Lett.* **103**, 64004 (2013).
- [47] E. Falcon, J.-C. Bacri, and C. Laroche, *Phys. Rev. Fluids* **2**, 102601(R) (2017).
- [48] S. Tatsumi, Y. Murayama, H. Hayakawa, and M. Sano, *J. Fluid Mech.* **641**, 521 (2009).
- [49] P. Yu, M. Schröter, and M. Sperl, *Phys. Rev. Lett.* **124**, 208007 (2020).
- [50] I. S. Aranson and J. S. Olafsen, *Phys. Rev. E* **66**, 061302 (2002).
- [51] J. Deseigne, S. Léonard, O. Dauchot, and H. Chaté, *Soft Matter* **8**, 5629 (2012).
- [52] J.-C. Tsai, F. Ye, J. Rodriguez, J. P. Gollub, and T. C. Lubensky, *Phys. Rev. Lett.* **94**, 214301 (2005).
- [53] E. Altshuler, J. M. Pastor, A. Garcimartín, I. Zuriguel, and D. Maza, *PLoS One* **8**, e67838 (2013).
- [54] C. Scholz, S. D'Silva, and T. Pöschel, *New J. Phys.* **18**, 123001 (2016).